PCCP

PAPER

View Article Online
View Journal | View Issue

Cite this: *Phys. Chem. Chem. Phys.*, 2022, **24**, 2656

Consistent characterization of the electronic ground state of iron(II) phthalocyanine from valence and core–shell electron spectroscopy†

Jonathan Laurent,[a] John Bozek,[b] Marc Briant,[c] Pierre Çarçabal,[a] Denis Cubaynes,[a] Aleksandar Milosavljević,[b] Ralph Püttner,[d] Niloufar Shafizadeh,[a] Marc Simon,[e] Benoît Soep[a] and Gildas Goldsztejn *[a]

Received 22nd October 2021,
Accepted 28th December 2021

DOI: 10.1039/d1cp04845g

rsc.li/pccp

We studied the iron(II) phthalocyanine molecule in the gas-phase. It is a complex transition organometallic compound, for which, the characterization of its electronic ground state is still debated more than 50 years after the first published study. Here, we show that to determine its electronic ground state, one needs a large corpus of data sets and a consistent theoretical methodology to simulate them. By simulating valence and core–shell electron spectra, we determined that the ground state is a ^3E_g and that the ligand-to-metal charge transfer has a large influence on the spectra.

1 Introduction

Since their discovery, metal phthalocyanines (MPc) have been widely studied because of their potential applications in a broad range of domains. From catalysis,[1] optoelectronics,[2] spintronics[3] to photodynamic therapy[4] to name a few. Among them, iron(II) phthalocyanine (FePc) is viewed as a potential molecular magnet.[5] However, despite numerous studies in the last six decades, the characterization of its electronic ground state (GS) remains highly controversial.

The Pc is an aromatic macrocycle that resembles to a porphyrin molecule, except for the substitution of aza-bridge carbons by nitrogen atoms. This therefore leads to the existence of two different types of nitrogen atoms, those surrounding the iron which are directly involved in the chemical bonds with the metal and the peripheric "aza-bridge" nitrogen atoms. In the center of Pc either a metal (Fe in the present case) or two hydrogens (free-based phthalocyanine) are located and the central ring is surrounded by four aromatic rings. The molecule is represented in Fig. 1.

The GS electronic properties of FePc are linked to the coupling of the Fe 3d orbitals with the π system of the phthalocyanine. This results in three electronic states with different distributions reflected in their spin states. For Fe II ferrous heme, the spins S = 0, 1 and 2 are possible due to the population of the d orbitals within the phthalocyanine cage.

One consensus is that the GS of FePc is in a spin-intermediate state with S = 1 based on measurements of its magnetic susceptibility as a function of the temperature performed by Dale *et al.*[6] and further reinforced by their Mössbauer-effect study[7] where the authors conclude the ground state to be of ^3E_g symmetry.

FePc belongs to the D_{4h} point group where the degeneracy of the five 3d orbitals is lifted into four levels b_{1g} (x^2-y^2), a_{1g} (z^2), b_{2g} (xy) and e_g, which is a doublet (xz, yz). With the exception of Thole *et al.*[8] who described FePc's GS as a quintet/triplet spin-mixed state, the literature also agrees on the fact that the b_{1g} orbital is too high in energy to be occupied. This is essential since the affinity of FePc to ligands is generally determined by the respective b_{1g} $(d_{x^2-y^2})$ and a_{1g} (d_{z^2}) populations. However, all possible arrangements for the three remaining orbitals can be found from experimental and/or computational studies.

The $^3A_{2g}$ GS with the configuration $|a_{1g}^2 b_{2g}^2 e_g^2 b_{1g}^0\rangle$ has been proposed by Stillman and Thomson[9] from magnetic circular dichroism measurements in solution. Note that we adopt a convention where the orbital ordering relates their relative energy. The same GS was predicted by Liao and Scheiner[10] and Sumimoto *et al.*[11] through density functional theory (DFT) studies. Recently, Greulich *et al.*[12] described FePc's GS as lying close to the transition between ^3E_g and $^3A_{2g}$ states after

[a] *Université Paris-Saclay, Institut des Sciences Moléculaires d'Orsay ISMO, UMR CNRS 8214, F-91405 Orsay, France. E-mail: gildas.goldsztejn@universite-paris-saclay.fr*
[b] *L'Orme des Merisiers, Synchrotron SOLEIL, Saint-Aubin, BP 48, F-91192 Gif-sur-Yvette Cedex, France*
[c] *Université Paris-Saclay, CEA, CNRS, LIDYL, 91191 Gif-sur-Yvette, France*
[d] *Fachbereich Physik, Freie Universität Berlin, Arnimallee 14, D-14195 Berlin, Germany*
[e] *Sorbonne Université, CNRS, Laboratoire de Chimie Physique-Matière et Rayonnement, LCPMR, F-75005 Paris Cedex 05, France*

† Electronic supplementary information (ESI) available. See DOI: 10.1039/d1cp04845g

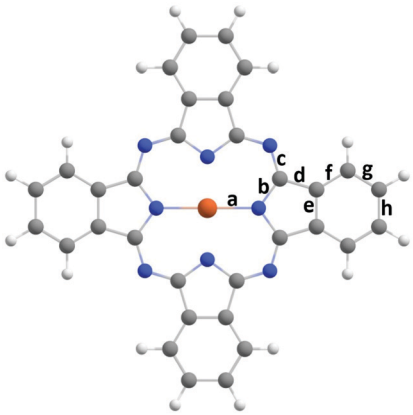

Fig. 1 Iron phthalocyanine possesses a D_{4h} symmetry and is composed of a porphyrin-like aromatic macrocycle where peripheric nitrogen atoms are in place of aza-bridge carbons. The macrocylce is surrounded by four aromatic rings and a Fe atom is located in its center. The labels "a" to "h" indicate different distances that will be referred to in the discussion.

performing X-ray absorption spectroscopy (XAS) and X-ray magnetic circular dichroism measurements at the Fe L-edge in thin films, supported by crystal-field multiplet calculations.

An early reference from Barraclough *et al.*[13] described the GS as $^3B_{2g}$ (*i.e.* $|e_g^4 b_{2g}^1 a_{1g}^1 b_{1g}^0\rangle$ configuration) after single crystal magnetic anisotropy measurements, followed by Brena and collaborators[14] who compared valence photoemission spectra and DFT calculations as well as in reference[15] where the authors performed XAS and XMCD spectra at the Fe L-edge of FePc adsorbed on Ag(001) and compared these with multiplet calculations.

As already mentioned, several articles found the GS to be a ^3E_g state,[7,16–21] either in the configuration $|b_{2g}^2 e_g^3 a_{1g}^1 b_{1g}^0\rangle$ or $|a_{1g}^2 e_g^3 b_{2g}^1 b_{1g}^0\rangle$. Finally, various references also conclude that the GS is a mixed state of ^3E_g–$^3B_{2g}$[22–24] or ^3E_g–$^3A_{2g}$[25–27] symmetries.

Such a diversity of results comes from diverse biases. Experimentally, it was found that for thin films the electronic state is highly dependent on the substrate (see for instance[12,28]) and, in particular, to charge transfer between the phthalocyanine and the substrate. An alternative approach is to probe MPc in thick films as performed by Bidermane *et al.*[21] who showed that the C 1s, N 1s and Fe 2p emission spectra were highly similar to those measured in the gas-phase. However, they did not arrive at the same conclusion as Brena *et al.*[14] who performed valence spectroscopy of FePc in the gas-phase and interpreted the GS on the basis of DFT calculations. Additionally, relying on one simulated spectrum only may not guarantee deriving the proper GS of such complex transition organometallic compound, independently of the theoretical method used. This is mainly due to the fact that the orbitals are quite close in energy and, therefore, a substantial amount of low-lying excited states can give qualitatively satisfying results for the simulation of the spectra.

From the theoretical viewpoint, it has been found that the GS determined by DFT calculations depends highly on the chosen functional and basis set, as in the ref. 29 where all simulated valence photoemission spectra are in fair agreement with the experimental one. Regarding the multiplet calculations, which have been shown to be well suited to calculate absorption spectra at the Fe $L_{2,3}$-edges,[30] many different sets of parameters have been reported for the crystal-field. Since these parameters are interdependent and often used to fit a particular data set, it is difficult to find parameters that would fit all the different experimental spectra.

In the present study, we decided to have a comprehensive experimental and theoretical approach to identify the GS of an isolated FePc molecule. We recorded outer-valence, shallow-core and core–shell photoemission spectra in the gas-phase and simulated our results with both DFT and multiplet calculations.

2 Methods

2.1 Experimental

The experiments were performed at the PLEIADES beamline[31,32] of the synchrotron radiation facility SOLEIL which is equipped with two undulators (HU256 and HU80) that allow to have access to a tunable photon energy between ≈10–1000 eV. This permits to probe a broad range of edges, from valence spectra close to ionization thresholds – the first IP of the molecule is at ≈6 eV – to C 1s and N 1s electrons (at ≈280 and 400 eV, respectively) and Fe 3p, 3s and 2p edges (≈60, 90 and 700 eV respectively). This allows recording an extensive set of spectra, in view of reaching a consistent characterization of the electronic GS able to reproduce the corpus of data. The spectra were recorded using the wide-angle lens VG-Scienta R4000 electron spectrometer installed at the beamline at a fixed position and the polarization vector of the incoming light was set at the so-called magic angle of 54.7° so that there is negligible influence of the photoelectron angular distribution on the photoionization cross sections. FePc has been graciously provided by Porphychem as a sublimated product. It is mostly free of synthesis pollutants. For the valence electron spectroscopy, data sets were recorded with photon energies between 52 and 110 eV and the electrons with a binding energy in the 6 to 20 eV range were detected with a step width of 20 meV. For the Fe 3p photoelectron spectra, we centered the binding energy of the electrons around 60 eV and used a step width of 100 meV; we varied the photon energy between 80 to 120 eV. We also measured resonant Auger spectra at the Fe $L_{2,3}$ edges using photon energies between 703 and 735 eV with a step width of 500 meV. The electrons were recorded in the binding-energy range of 5 to 110 eV with a step width of 200 meV. Such a large binding energy range allows extracting most of the emitted electrons after resonant Auger decays and give, after integration over all binding energies, access to a partial electron yield (PEY) spectrum, which is comparable to absorption spectra. The total experimental resolution, composed of the convolution between the monochromator and spectrometer resolutions, was chosen to represent a good compromise between intensity of the signal and its resolution. In case of the valence spectra the total

instrumental resolution amounted ≈60 meV, while in case of the Fe 3p XPS spectra it was ≈500 meV and for the core resonant Auger spectra where the spectral contributions are inherently large, it was ≈600 meV for the photon bandwidth.

The molecules were evaporated at ≈700 K under vacuum in a home-made oven designed to fit the Scienta's specifications and both the temperature of the oven and pressure in the interaction chamber were monitored during the data acquisition to ensure stable target densities. The oven was set on a 3D-axis manipulator and its position was optimized on the signal.

2.2 DFT calculations

The DFT calculations were performed with the Gaussian 16 software package.[33] The structures have been optimized using the hybrid Becke 3-parameter, Lee, Yang and Parr (B3LYP) and the B97D3 functionals. We performed two sets of calculations with and without imposing the D_{4h} symmetry. We verified that the electronic structures as well as the c^2 coefficients for the molecular orbitals and their energies were almost identical in both cases. Therefore, to enable the comparison with both our multiplet calculations and the literature, we retained the results of the imposed-symmetry calculations in the following. We used different basis sets in order to evaluate their effect on the optimized structure and found that the B3LYP functional was robust with the choice of the basis set, *i.e.* whatever the chosen basis set we found (i) very comparable geometric structure, (ii) that the triplet state is the most stable electronic structure, followed by the quintuplet (≈0.9 eV higher) and the singlet (≈1.3 eV higher in energy). In the following, we present the results with the correlation-consistent polarized triple-zeta (cc-pVTZ) basis set used for all atoms. To simulate the valence photoelectron (PE) spectra, we calculated the partial and total density of states (DOS) by using the optimized structure. The result using the B3LYP functional matches slightly better the experimental spectrum than with the B97 functional, as can be seen in the Fig. S2 of the ESI.† The partial DOS (PDOS) were calculated using the keyword pop = full iop(3/33 = 1,3/36 = −1) in Gaussian on a single point calculation on the optimized structure and the percentages of each groups of atoms to the molecular orbitals were calculated using the Mulliken population analysis and the software GaussSum.[34] To simulate the PE spectra, we followed the procedure described by Brena *et al.*[14] and used the Gelius model[35] which consists in weighing each atomic orbital of the PDOS by the atomic subshell photoionization cross sections; for these cross sections we used the theoretical values from Yeh and Lindau.[36,37] Finally, due to the hybrid character of the sp orbitals of C and N atoms, we decided to weight their contributions in the PDOS by the population given in the DFT calculation instead of separating them into 2s and 2p contributions as in ref. 14. To simulate the PE spectra, we convoluted the theoretical peaks using Gaussian functions with four different full width at half maximum (FWHM) according to their binding energies, *i.e.* FWHM = 135 meV for energies below 6.5 eV, FWHM = 300 meV for energies between 6.5 and 8.2 eV, FWHM = 500 meV for 8.2 ≤ E ≤ 9.5 eV and FWHM = 1.5 eV above 9.5 eV. This allows to take into account that at higher energies the contributions of 2-holes 1-electron final states corresponding to simultaneous ionization and excitation become more important.

2.3 Multiplet calculations

In Fig. 2, we described the crystal-field parameters in a single-electron picture. In a free ion, all 3d orbitals have the same energy. In contrast to this, in the O_h (octahedral) symmetry there is a splitting of the d-level into two groups of orbitals: e_g, which is a doublet comprising the z^2 and $x^2 - y^2$ orbitals, and t_{2g}, which is a triplet constituted by the xy, xz and yz orbitals. In this symmetry, the only important parameter is $10Dq$ which relates to the energy difference between the e_g and t_{2g} orbitals. When the symmetry is further lowered to a tetragonal symmetry D_{4h}, the orbitals are split into 4 levels, namely b_{1g} ($x^2 - y^2$), a_{1g} (z^2), b_{2g} (xy) and e_g, which is doubly degenerated (xz, yz). To describe the crystal field, two more parameters are needed, the so-called Ds and Dt. The four levels are linked by a set of formulas:[30,38,39]

$$E_{b_{1g}} = +6Dq + 2Ds - Dt(x^2 - y^2)$$

$$E_{a_{1g}} = +6Dq - 2Ds - 6Dt(z^2)$$

$$E_{e_g} = -4Dq - Ds + 4Dt(xz, yz)$$

$$E_{b_{2g}} = -4Dq + 2Ds - Dt(xy)$$

However, these energy shifts are only correct for a single electron in the d-shell because the formulas do not take into account the coupling between the electrons, *i.e.* the situation is much more complex when the four levels are occupied by several electrons.

To perform the multiplet calculations and simulate the PEY and PE spectra, we used the Charge Transfer Multiplet program for X-ray Absorption Spectroscopy (CTM4XAS version 5.5)[40] and for the determination of the ground state, we used the version

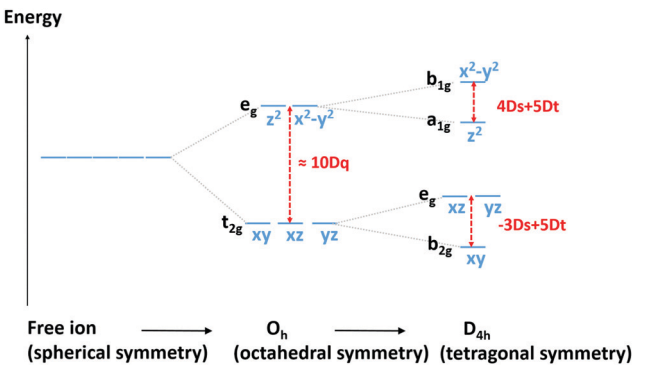

Fig. 2 Representation of the symmetry effect on the 3d orbitals. For a spherical symmetry the 5 3d orbitals have the same energy, in an octahedral symmetry (O_h), there is a degeneracy splitting into two different levels e_g and t_{2g} separated in energy by ≈$10Dq$. When the symmetry is further lowered to the D_{4h} point group, the d orbitals are further separated into 4 different levels named b_{1g}, a_{1g}, e_g and b_{2g}. In this case, two distorsion parameters Ds and Dt describe the splitting between the levels.

1.9 of the CTM4DOC[41] (differential orbital covalency) software. Depending on the chosen parameters, the CTM4XAS program allows to take into account the core-hole induced effects on the electronic structure, which are neglected when considering the core/inner-shell excitation or ionization as a single electron process. These effects include its potential, the spin–orbit coupling, the core-hole induced charge transfer effect, the core and valence holes exchange and multipole interactions.[40] To further detail these multiplet calculations, the Hamiltonian is described as a sum of three contributions, namely (i) a free ion Hamiltonian regrouping the kinetic energy of the electrons, the electron–nuclear, the electron–electron and the spin–orbit interactions, (ii) a crystal field Hamiltonian and (iii) an hybridization Hamiltonian. Note that the contributions (ii) and (iii) characterize the ligand field experienced by the centered metal atom. Once the Hamiltonian is described, the wavefunction can be calculated and further projected on a basis consisting of all possible configurations, each affiliated with a coefficient α_i (eigenvalues). The numbers given on page 6 in front of each configuration are the α_i^2 values for the 6 dominant configurations ($\sum \alpha_i^2 = 1$, if all possible configurations are taken into account).

A large number of parameters' combinations and approaches can be found in the literature to match various spectra. Here we chose the strategy to use the same parameters to fit all spectra (L-edge PEY and PE spectra and M-edge PE spectrum). We reduced the Slater radial integrals to 68% of their Hartree–Fock value which is in agreement with the ref. 6, 12, 24, 25 and 27. This lowering is related to the fact that the bonding between Fe and its neighbours is partly covalent and partly ionic. In general, when this factor is comprised between 0.7 and 0.9 the bond is considered predominantly with an ionic character, while when it is between 0.5 and 0.6, it has a covalent character. Here, we are in an intermediate situation adding complexity to the characterization of the GS.

The optical parameters found as a best fit for our experimental spectra are $10Dq$ = 2.66 eV, Ds = 0.625 eV and Dt = 0.234 eV which are in relatively close agreement with the ref. 12, 18, 23 and 25.

To find the accurate charge transfer parameters, we fixed the charge transfer energy to Δ = 1.63 eV. This value comes from the interpretation of a ligand-to-metal charge transfer band in the visible absorption spectrum of gas-phase FePc[42] and is consistent with the interpretation of the absorption spectrum of FePc in dichlorobenzene.[9,11]

To determine the values of U_{pd}, the core-hole potential, and U_{dd}, the Hubbard value, we fitted our X-ray PE spectra. It resulted in the charge transfer parameters: Δ = 1.3 eV, U_{dd} = 5 eV and U_{pd} = −2 eV. Δ describes the energy needed to transfer one electron from the ligand to the metal atom and U_{dd} as well as U_{pd} represent the Coulomb energy between two 3d electrons as well as a 3d electron and a 2p core electron, respectively.

Finally, we used T(b1) = T(a1) = 2 eV and T(b2) = T(e) = 1 eV, where T are the metal–ligand hopping integrals.

Although the discussion of the influence of the substrate on the electron spectra, as compared to the gas-phase measurements, is out of the scope of the present study, we tried to fit our data with the parameters given in the works of Greulich *et al.*[12] and Stepanow *et al.*[23] that deal with films of FePc on GeS(100) and Au(111) substrates respectively. We observed that for the first one cited, the agreement with our spectra is only slightly worse than with the parameters used in the present study, which goes along with the choice of Greulich *et al.* for this substrate as to avoid interactions with FePc. There is, however, a clear difference when using the parameters used in Stepanow *et al.* where, as they noted, the spin of the substrate couples with the Fe ion.

3 Results and discussion

3.1 Valence spectroscopy and DFT calculations

The experimental spectrum taken at $h\nu$ = 55.64 eV is shown in Fig. 3 (red dots), along with the simulated DOS (black line) and the individual atomic intensities are plotted below as sticks. The simulated spectrum has been normalized over the most intense experimental point. The other features, marked by a star, are dominated by water contribution (blue stars), other peaks (red stars) are either due to other contaminants of the sample or to simultaneous ionized and excited states which are not accounted for in our simulation. We show in Fig. S1 of the ESI,† the experimental spectrum of the background taken in the same experimental conditions, *i.e.* oven on but without the FePc.

The good agreement between simulated and experimental spectra is an indication that the structure of FePc is properly reproduced by the DFT calculations. Indeed, in Table 1, we summarized the values of our calculations for the distances labeled from "a" to "h" in Fig. 1 and compared them to experimental values obtained with X-ray diffraction.[43] The values presented in Sumimoto *et al.*[11] and Brena *et al.*[14] are also displayed in the table and show a comparable agreement

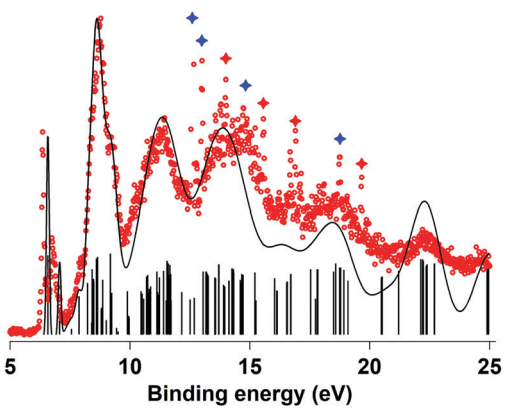

Fig. 3 Valence photoelectron spectrum measured at $h\nu$ = 55.64 eV (red dots) along with a simulation using the density of states which is represented as a black solid line. The intensities of each individual molecular orbital is indicated by the stick lines. The blue stars indicate contributions of the background which is mostly due to water contributions. Red stars correspond to feature that may belong either to other contaminants of the sample or to simultaneous ionized and excited states not accounted for by the DOS simulation.

Table 1 Summary of the distances "a" to "h" in Fig. 1 given for the optimized structures of the present work, of Sumimoto *et al.*[11] and of Brena *et al.*,[14] as well as the experimental values from ref. 43. δr is the average deviation to the experimental values (see text) and Δr_{max} is the maximum deviation between a single calculated and experimental values, both in Å

	Expt.[43] (Å)	This work	Sumimoto *et al.*[11]	Brena *et al.*[14]
a	1.927	1.948	1.941	1.947
b	1.378	1.374	1.379	1.381
c	1.322	1.318	1.323	1.322
d	1.450	1.452	1.454	1.456
e	1.395	1.401	1.396	1.405
f	1.392	1.391	1.406	1.396
g	1.390	1.388	1.393	1.394
h	1.394	1.403	1.409	1.409
δr	—	0.006	0.007	0.008
Δr_{max}	—	0.021	0.015	0.020

with our values. The two last lines of the table are the average deviation to the experimental values calculated as $\delta r = \sum_{i=''a''}^{i=''h''} \frac{|r_{i,exp} - r_{i,DFT}|}{8}$ and Δr_{max} is the maximum deviation between calculated and experimental values, both in Å.

Although the three DFT calculations presented in Table 1 show comparable agreements with the experimental values and geometric structures being very close to each other, they predict three different descriptions of the electronic GS. We find the GS to be ^3E_g ($|b_{2g}^2 e_g^3 a_{1g}^1 b_{1g}^0\rangle$), Sumimoto *et al.*[11] found it to be a $^3A_{2g}$ ($|b_{2g}^2 e_g^2 a_{1g}^2 b_{1g}^0\rangle$), while Brena *et al.*[14] gave a $^3B_{2g}$ ($|b_{2g}^1 e_g^4 a_{1g}^1 b_{1g}^0\rangle$) GS. The origin of these differences in the ground-state configurations is probably due to the fact that the energy levels of the three lowest d orbitals (according to the present calculation, the b_{2g} orbital is the lowest in energy, but it is separated by only 0.4 eV and 0.44 eV from the e_g and the a_{1g} orbital, respectively, while the b_{1g} orbital is 2.65 eV higher in energy) are close to each other so that different theoretical approaches may result in different sequences for the three lowest levels.

Moreover, in agreement with Sumimoto *et al.*,[11] our DFT calculations give similar optimized geometrical structures for the singlet and quintuplet states or even by using a different functional, namely the B97D3 (see Table S1 in the ESI†), as those given in Table 1. Furthermore, all calculations give a reasonably good agreement with the experiment spectrum when simulating their DOS spectra (see Fig. S2 and S3 of the ESI†). This is also in agreement with Marom *et al.*[29] who performed DFT calculations with many different functional and basis sets. In detail, they found for MgPc and FePc that the various simulated DOS spectra match well the valence spectra, although the obtained GS were different.

To summarize, we found that the simulated DOS spectrum related to the DFT calculation done with the B3LYP functional gives the best agreement with the valence spectra, compared to the B97D3 functional. It also describes the triplet state as being more stable than the quintuplet and singlet electronic ones. However, since the agreement of DOS spectra stemming from all the above-mentioned DFT calculations with our experimental spectrum is relatively good, it did not seem advisable to us to simply rely on this result and chose to confirm it with the use of shallow-core and core–shell spectroscopies.

3.2 Core-hole spectroscopy and multiplet calculations

To determine the electronic structure of the d-orbitals, it is more efficient to probe it directly at the Fe site. This can be done by core electron emission.

In Fig. 4, we plotted the PEY measured around the $L_{2,3}$-edges as red dots. The black solid line is the simulated spectrum using the charge transfer and crystal field parameters described above. To compare with the experimental spectrum, we used two Lorentzian functions of 0.1 (L_3) and 0.6 eV (L_2) and convolved by a Gaussian function of 0.6 eV to simulate the experimental resolution. The result of our simulation is in fairly good agreement with the experimental spectrum. In particular, it reproduces well the shoulder at low binding energy ($\approx$706 eV) and the spin–orbit energy difference between L_2 and L_3 is also well reproduced. The main discrepancy resides in the tail region which may be due to vibrational progressions (see for instance ref. 44).

We did not measure the Fe 2p photoelectrons spectrum of FePc, however in Fig. 5, the experimental spectrum from Bidermane *et al.*,[21] reproduced with permission, for thick films (red dots) was used to test the quality of our parameters on these data as well. The result of our simulation is displayed on the same graph as a black solid line and the intensities of each contribution is shown below as black sticks. To match the experimental spectrum, we convoluted the spectrum with two Lorentzian functions of 0.1 and 0.6 eV and a Gaussian function of 0.3 eV. The agreement with the PE spectrum is very good and reproduces well the shoulder at $\approx$707 eV. In contrast to the cited reference, where the authors included a final state different from the initial one in order to better fit their results, we chose to find a consistent set of parameters that suits all shallow-core and core–shell spectra. In Fig. 6 we present the experimental PE spectrum of the shallow-core level Fe 3p as red

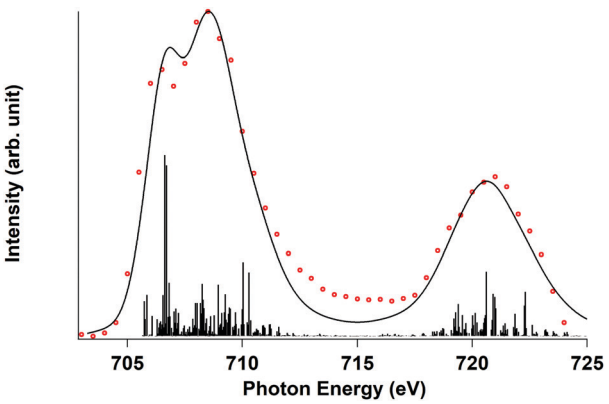

Fig. 4 The partial electron yield (red dots) in the photon energy range from 703 to 724.5 eV. The parameters used to plot the simulated XAS spectrum (black solid line) are detailed in the main text. The intensities of the simulated spectrum are indicated with black sticks.

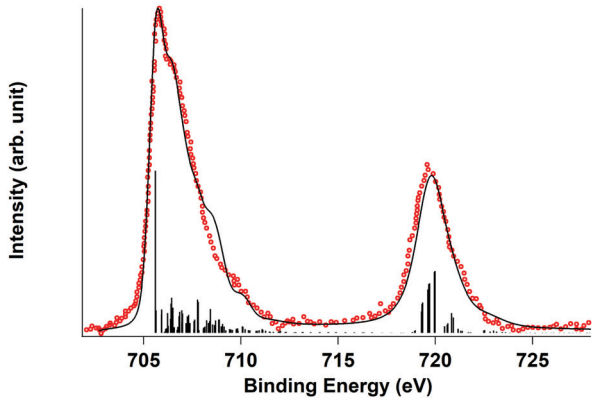

Fig. 5 XPS spectrum at the Fe $L_{2,3}$ edges measured (red dots) by Bidermane *et al.*[21] and reproduced here to test our CTM parameters. The result of the calculation is plotted as a black solid line and the intensities of each contribution are plotted as stick lines underneath.

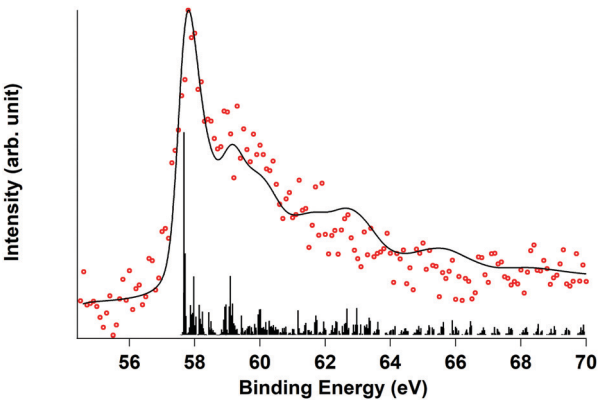

Fig. 6 Fe 3p XPS spectrum measured at $h\nu$ = 100 eV. The red points correspond to the experimental spectrum, while the black solid line is the calculated spectrum. The individual theoretical intensities are plotted as stick lines below the graph.

dots and the simulated spectrum by a black solid line. Here, we also find a very good match between our CTM calculations, which is convoluted with Lorentzian functions of 0.1 and 0.4 eV of FWHM and a Gaussian function of 0.2 eV, and the experimental spectrum. The Fe 3p photoelectron spectrum, which to the best of our knowledge has never been published before, turned out to be particularly important to determine the parameters that describe the ligand field splitting.

Finally, by projecting the result of the GS onto pure symmetries, we can define it as a linear combination of various configurations[41] as:

$$\begin{aligned}\mathrm{GS} &= 0.457 \times \left|b_{2g}^2 e_g^3 a_{1g}^1 b_{1g}^0\right\rangle + 0.113 \times \left|b_{2g}^1 e_g^4 a_{1g}^1 b_{1g}^0\right\rangle \\ &+ 0.092 \times \left|b_{2g}^1 e_g^3 a_{1g}^2 b_{1g}^0\right\rangle \\ &+ 0.102 \times \left|b_{2g}^2 e_g^3 a_{1g}^1 b_{1g}^1\right\rangle + 0.098 \times \left|b_{2g}^2 e_g^3 a_{1g}^2 b_{1g}^0\right\rangle \\ &+ 0.032 \times \left|b_{2g}^1 e_g^3 a_{1g}^2 b_{1g}^1\right\rangle\end{aligned}$$

where the last two lines correspond to the effect of charge transfer. Therefore the ground state is predominantly of ^3E_g symmetry, as was found from our DFT calculation. In both approaches we found the same orbital order, *i.e.* the b_{2g} orbital is the lowest in energy, followed by e_g, a_{1g} and b_{1g}. We find charge transfer to be responsible for ~26% of the GS, which is a much larger contribution than that reported in ref. 12.

As in the article of Carlotto *et al.*,[45] our calculations show that the energy levels of the three different symmetries ^3E_g, $^3B_{2g}$ and $^3A_{2g}$ are close to each other. However, we found differences in the sequence of states and obtained splittings. In detail, in the ref. 45, the GS was found to be the $^3A_{2g}$ state separated to the ^3E_g and $^3B_{2g}$ states by 0.05 and 0.06 eV respectively. In the present study the ^3E_g is lower in energy by 0.14 and 0.37 eV than the $^3B_{2g}$ and $^3A_{2g}$ states, respectively.

To further corroborate our assessment from the CTM calculations, we also simulated the Fe 2p XAS and XPS spectra for the states $^3B_{2g}$ and $^3A_{2g}$. The simulated XAS and XPS spectra of the $^3A_{2g}$ state do not agree with the experimental spectra. For the $^3B_{2g}$ state, the situation is more complex since in this case the simulated XAS and Fe 3p XPs spectra of the $^3B_{2g}$ state are very similar to the ^3E_g state, which we identified as ground state. In contrast to this, the 2p XPS spectra (Fig. S4 of the ESI†) shows clear differences in the energy range from 707 to 708 eV, with the simulated spectrum of the ^3E_g state being better in line with the experimental spectrum. Secondly, the intensity ratio between the L_2 and L_3 edges is poorly reproduced for the $^3B_{2g}$ state. In summary, only the simulated spectra of the ^3E_g state match all experimental data. This is an additional evidence that one needs a consistent analysis of different data sets in order to identify the electronic GS of such complex systems.

The configuration given by the CTM and the DFT calculations, respectively $|b_{2g}^{1.73} e_g^{3.13} a_{1g}^{1.25} b_{1g}^{0.15}\rangle$ and $|b_{2g}^{1.97} e_g^{2.93} a_{1g}^{1.01} b_{1g}^{0.62}\rangle$, compare well to each other. In case of the DFT calculation, the result shows that 6.53 electrons are located on the Fe 3d orbitals, this is also in relative agreement with the 6.26 electrons found by the CTM calculation. However, a difference resides in the fact that in case of the DFT calculation almost all of the charge is transferred from the lone pairs of the N atoms to the b_{1g} orbital, while it is predicted by the CTM calculation to be evenly distributed between a_{1g} and b_{1g} orbitals. This difference between both results probably lies in the fact that for the latter, we define the metal atom in a certain degree of oxidation (+2 in the present study) and the molecular environment is considered only as a perturbation to the free ion's Hamiltonian.

4 Conclusion

We have performed PE and PEY measurements at various edges of the FePc molecule and complemented them by DFT and CTM calculations in order to simulate these spectra and, in turn, identify the GS of the isolated molecule. Our approach consisted in finding a consistent description able to reproduce the corpus of available data. We observed that valence

photoelectron spectroscopy is less sensitive to the exact GS, since different structures and spin-states can provide simulated spectra that all reasonably match the experimental one. This result can readily be understood by the fact that with valence photoelectron spectroscopy, the entire molecule is probed. In contrast to this, inner-shell PE spectra that are direct probes of the centered-metal atom, which is a crucial step to identify the GS. By comparing the PE spectra at the 2p and 3p edges as well as the PEY around the 2p resonances and by fitting them with the same crystal field and charge transfer parameters, we were able to identify that the GS of FePc to be of ^3E_g symmetry and find that the charge transfer between the Fe atom and its N atoms neighbours has to be taken into account.

Author contributions

N. S., B. S., M. S. and G. G. conceived and planned the experiment, J. B., M. B., P. C., D. C., A. M., N. S., B. S. and G. G. performed the experiment, J. L. and G. G. analyzed the data, G. G. performed the theoretical simulations, J. L., N. S., M. S., B. S. and G. G. interpreted the findings, J. L., R. P., N. S., B. S. and G. G. drafted the manuscript and all authors discussed the results and contributed to the final manuscript.

Conflicts of interest

There are no conflicts to declare.

Acknowledgements

G. G. wants to thank Prof. Dr Frank de Groot for invaluable help on the usage of the CTM softwares. We are thankful to Dr Habermeyer from Porphychem for providing a sample of sublimated FePc.

Notes and references

1 C. C. Leznoff and A. B. P. Lever, *Phthalocyanines, Properties and Applications*, VCH, New York, 1989, vol. 4.
2 K. Walzer, B. Maennig, M. Pfeiffer and K. Leo, *Chem. Rev.*, 2007, **107**, 1233–1271.
3 N. Domingo, E. Bellido and D. Ruiz-Molina, *Chem. Soc. Rev.*, 2012, **41**, 258–302.
4 E. Reddi, G. L. Castro, R. Biolo and G. Jori, *Br. J. Cancer*, 1987, **56**, 597–600.
5 N. Ishikawa, in *Phthalocyanine-Based Magnets*, ed. J. Jiang, Springer Berlin Heidelberg, Berlin, Heidelberg, 2010, pp. 211–228.
6 B. W. Dale, R. J. P. Williams, C. E. Johnson and T. L. Thorp, *J. Chem. Phys.*, 1968, **49**, 3441–3443.
7 B. W. Dale, R. J. P. Williams and C. E. Johnson, *J. Chem. Phys.*, 1968, **49**, 3445–3449.
8 B. T. Thole, G. V. der Laan and P. H. Butler, *Chem. Phys. Lett.*, 1988, **149**, 295–299.
9 M. J. Stillman and A. J. Thomson, *J. Chem. Soc., Faraday Trans. 2*, 1974, 790–804.
10 M.-S. Liao and S. Scheiner, *J. Chem. Phys.*, 2001, **114**, 9780–9791.
11 M. Sumimoto, Y. Kawashima, K. Hori and H. Fujimoto, *Dalton Trans.*, 2009, 5737–5746.
12 K. Greulich, M. Trautmann, A. Belser, S. Bölke, R. Karstens, P. Nagel, S. Schuppler, M. Merz, A. Chassé, T. Chassé and H. Peisert, *J. Phys. Chem. C*, 2021, **125**, 6851–6861.
13 C. G. Barraclough, R. L. Martin, S. Mitra and R. C. Sherwood, *J. Chem. Phys.*, 1970, **53**, 1643–1648.
14 B. Brena, C. Puglia, M. de Simone, M. Coreno, K. Tarafder, V. Feyer, R. Banerjee, E. Göthelid, B. Sanyal, P. M. Oppeneer and O. Eriksson, *J. Chem. Phys.*, 2011, **134**, 074312.
15 S. Stepanow, A. L. Rizzini, C. Krull, J. Kavich, J. C. Cezar, F. Yakhou-Harris, P. M. Sheverdyaeva, P. Moras, C. Carbone, G. Ceballos, A. Mugarza and P. Gambardella, *J. Am. Chem. Soc.*, 2014, **136**, 5451–5459.
16 P. Coppens, L. Li and N. J. Zhu, *J. Am. Chem. Soc.*, 1983, **105**, 6173–6174.
17 G. Filoti, M. D. Kuz'min and J. Bartolomé, *Phys. Rev. B: Condens. Matter Mater. Phys.*, 2006, **74**, 134420.
18 P. S. Miedema, S. Stepanow, P. Gambardella and F. M. F. de Groot, *J. Phys.: Conf. Ser.*, 2009, **190**, 012143.
19 M. D. Kuz'min, R. Hayn and V. Oison, *Phys. Rev. B: Condens. Matter Mater. Phys.*, 2009, **79**, 024413.
20 T. Kroll, R. Kraus, R. Schönfelder, V. Yu, O. V. Molodtsova, P. Hoffmann and M. Knupfer, *J. Chem. Phys.*, 2012, **137**, 054306.
21 I. Bidermane, J. Lüder, R. Totani, C. Grazioli, M. de Simone, M. Coreno, A. Kivimäki, J. Åhlund, L. Lozzi, B. Brena and C. Puglia, *Phys. Status Solidi B*, 2015, **252**, 1259–1265.
22 P. A. Reynolds and B. N. Figgis, *Inorg. Chem.*, 1991, **30**, 2294–2300.
23 S. Stepanow, P. S. Miedema, A. Mugarza, G. Ceballos, P. Moras, J. C. Cezar, C. Carbone, F. M. F. de Groot and P. Gambardella, *Phys. Rev. B: Condens. Matter Mater. Phys.*, 2011, **83**, 220401.
24 J. Fernández-Rodríguez, B. Toby and M. van Veenendaal, *Phys. Rev. B*, 2015, **91**, 214427.
25 P. S. Johnson, J. M. García-Lastra, C. K. Kennedy, N. J. Jersett, I. Boukahil, F. J. Himpsel and P. L. Cook, *J. Chem. Phys.*, 2014, **140**, 114706.
26 J. Bartolomé, F. Bartolomé, A. I. Figueroa, O. Bunau, I. K. Schuller, T. Gredig, F. Wilhelm, A. Rogalev, P. Krüger and C. R. Natoli, *Phys. Rev. B: Condens. Matter Mater. Phys.*, 2015, **91**, 220401.
27 C. R. Natoli, P. Krüger, J. Bartolomé and F. Bartolomé, *Phys. Rev. B*, 2018, **97**, 155139.
28 H. Peisert, J. Uihlein, F. Petraki and T. Chassé, *J. Electron Spectrosc. Relat. Phenom.*, 2015, **204**, 49–60.
29 N. Marom and L. Kronik, *Appl. Phys. A: Mater. Sci. Process.*, 2009, **95**, 165–172.
30 F. de Groot and A. Kotani, *Core Level Spectroscopy of Solids. Advances in Condensed Matter Science*, CRC Press, 2008.
31 https://www.synchrotron-soleil.fr/en/beamlines/pleiades.

32 C. Miron, C. Nicolas, O. Travnikova, P. Morin, Y. Sun, F. Gel'mukhanov, N. Kosugi and V. Kimberg, *Nat. Phys.*, 2012, **8**, 135–138.
33 M. J. Frisch, G. W. Trucks, H. B. Schlegel, G. E. Scuseria, M. A. Robb, J. R. Cheeseman, G. Scalmani, V. Barone, G. A. Petersson, H. Nakatsuji, X. Li, M. Caricato, A. V. Marenich, J. Bloino, B. G. Janesko, R. Gomperts, B. Mennucci, H. P. Hratchian, J. V. Ortiz, A. F. Izmaylov, J. L. Sonnenberg, D. Williams-Young, F. Ding, F. Lipparini, F. Egidi, J. Goings, B. Peng, A. Petrone, T. Henderson, D. Ranasinghe, V. G. Zakrzewski, J. Gao, N. Rega, G. Zheng, W. Liang, M. Hada, M. Ehara, K. Toyota, R. Fukuda, J. Hasegawa, M. Ishida, T. Nakajima, Y. Honda, O. Kitao, H. Nakai, T. Vreven, K. Throssell, J. A. Montgomery, Jr., J. E. Peralta, F. Ogliaro, M. J. Bearpark, J. J. Heyd, E. N. Brothers, K. N. Kudin, V. N. Staroverov, T. A. Keith, R. Kobayashi, J. Normand, K. Raghavachari, A. P. Rendell, J. C. Burant, S. S. Iyengar, J. Tomasi, M. Cossi, J. M. Millam, M. Klene, C. Adamo, R. Cammi, J. W. Ochterski, R. L. Martin, K. Morokuma, O. Farkas, J. B. Foresman and D. J. Fox, *Gaussian 16 Revision C.01*, Gaussian Inc., Wallingford, CT, 2016.
34 N. M. O'boyle, A. L. Tenderholt and K. M. Langner, *J. Comput. Chem.*, 2008, **29**, 839–845.
35 U. Gelius, *J. Electron Spectrosc. Relat. Phenom.*, 1974, **5**, 985–1057.
36 J. Yeh and I. Lindau, *At. Data Nucl. Data Tables*, 1985, **32**, 1–155.
37 J. Yeh, *Atomic Calculation of Photoionization Cross-Sections and Asymmetry Parameters*, Gordon and Breach Science Publishers, Langhorne, PE (USA), 1993.
38 P. Zimmermann, N. Bouldi, M. O. J. Y. Hunault, M. Sikora, J. Ablett, J.-P. Rueff, B. Lebert, P. Sainctavit, F. M. F. de Groot and A. Juhin, *J. Electron Spectrosc. Relat. Phenom.*, 2018, **222**, 74–87.
39 S. L. Reddy, T. Endo and G. S. Reddy, *Electronic (Absorption) Spectra of 3d Transition Metal Complexes*, INTECH Open Access Publisher, 2012.
40 E. Stavitski and F. M. F. de Groot, *Micron*, 2010, **41**, 687–694.
41 M. U. Delgado-Jaime, K. Zhang, J. Vura-Weis and F. M. F. de Groot, *J. Synchrotron Radiat.*, 2016, **23**, 1264–1271.
42 L. Edwards and M. Gouterman, *J. Mol. Spectrosc.*, 1970, **33**, 292–310.
43 J. F. Kirner, W. Dow and W. R. Scheidt, *Inorg. Chem.*, 1976, **15**, 1685–1690.
44 C. Kolczewski, R. Püttner, O. Plashkevych, H. Ågren, V. Staemmler, M. Martins, G. Snell, A. S. Schlachter, M. Sant'Anna, G. Kaindl and L. G. M. Pettersson, *J. Chem. Phys.*, 2001, **115**, 6426–6437.
45 S. Carlotto, M. Sambi, F. Sedona, A. Vittadini and M. Casarin, *Nanomaterials*, 2021, **11**, 54.